Eur. Phys. J. B **28**, 223–230 (2002)
DOI: 10.1140/epjb/e2002-00224-8

THE EUROPEAN PHYSICAL JOURNAL B

A detailed Raman study on thin single-wall carbon nanotubes prepared by the HiPCO process

A. Kukovecz[1,a], Ch. Kramberger[1], V. Georgakilas[2], M. Prato[2], and H. Kuzmany[1]

[1] Institut für Materialphysik, University of Vienna, Strudlhofgasse 4., 1090 Wien, Austria
[2] Dipartimento di Scienze Farmaceutiche, University of Trieste, Piazzale Europa 1., 34127 Trieste, Italy

Received 5 February 2002 / Received in final form 3 April 2002
Published online 19 July 2002 –

Abstract. The Raman spectrum of single wall carbon nanotubes (SWNTs) prepared by high pressure CO decomposition (HiPCO process) has been recorded at nine excitation laser energies ranging from 1.83 eV to 2.71 eV. The characteristic nanotubes features: G band, D band and radial breathing mode (RBM) have been analyzed and compared to those of an arc discharge SWNT material of similar diameter. A strong Breit-Wigner-Fano type (metallic) contribution to the G band was found in the spectra measured with green lasers, while spectra measured with red lasers indicate resonances of semiconducting SWNTs. Analysis of the energy dependence of the position of the D band revealed sinusoid oscillations superimposed on a linear trend. The validity of full DOS calculations for HiPCO materials has been confirmed by a match found between the estimated spectral contribution of metallic SWNTs as calculated from the components of the measured G band and as predicted by the (n, m) indexes of the major scatterers of DOS simulations. The RBM region of the HiPCO spectrum is more complex than usually observed for SWNTs. The analysis performed with a Gaussian distribution and improved fitting parameters leads to a mean diameter and variance of 1.05 nm and 0.15 nm, respectively. A bimodal Gaussian distribution had little influence on the error sum but reduced the standard error slightly. The major spectral features of the RBM could be interpreted using available resonance Raman theory.

PACS. 61.46.+w Nanoscale materials: clusters, nanoparticles, nanotubes, and nanocrystals – 78.30.-j Infrared and Raman spectra – 63.20.Dj Phonon states and bands, normal modes, and phonon dispersion

1 Introduction

Single-wall carbon nanotubes (SWNTs) have been in the focus of scientific attention ever since their discovery in 1993 [1]. Most often visualized as rolled-up graphite sheets with diameters between 0.5–2 nm and lengths of several μm, these unique structures are expected to become important tools of nanoindustry in the near future. The properties of SWNTs are determined by the *Hamada vector*, the folding vector along which the graphite sheet is rolled up into itself. It is widely accepted to refer to SWNTs by the (n, m) indexes of this vector – often denoted as the "helicity" of the tube. The (n, n) or "armchair" tubes are always metallic, while the $(n, 0)$ "zigzag" and (n, m) "chiral" tubes are metallic or at least quasi-metallic with a very narrow gap if $(n-m)$ mod $3 = 0$ and semiconducting otherwise.

Very recently, the two traditional batch-based SWNT synthesis methods, d.c. arc discharge [2] and laser ablation [3] have been challenged by a new technique, the high pressure gas-phase decomposition of CO (HiPCO process) [4]. Since HiPCO is a continuous flow process, it excels in scalability and product yield as well as in SWNT-to-amorphous carbon ratio, while somewhat lagging behind with respect to reproducibility concerning the width of diameter distribution and the amount of leftover metal catalyst particles. Another advantage of HiPCO tubes is their better accessibility for purification as at least the metallic particles can be etched away more easily. The diameter of the HiPCO product can be varied over a broad range by tuning feedstock composition and the amount of catalyst applied. The reported average diameter of 1.2 nm is smaller than the corresponding typical arc discharge and laser ablation values. The thinnest SWNTs (0.7 nm) observed in bulk carbon phase up till now were also obtained by CO decomposition [4]. Summarizing, the HiPCO process has the potential to become an important tool of nanotube science in the next 3–5 years.

Raman spectroscopy has been demonstrated to be a key technique for the characterization of SWNTs. This is due to the strong resonance enhancement of the scattering cross section and a photoselective response of the

[a] e-mail: akos@ap.univie.ac.at

radial breathing mode with respect to tube diameters. Application of this technique has been demonstrated repeatedly [5–7]. A quantitative application of the analysis needs a refined treatment as it was shown recently [8].

Even though resonance Raman spectroscopy is now well-documented for determining the diameter distribution of SWNT its reported applications to HiPCO SWNTs are only qualitative, being aimed primarily towards characterizing sample purity [9] and electrochemical behavior [10]. On account of the expected technical importance of the material a quantitative analysis of the material is desirable. In this contribution, we present the first detailed Raman study involving nine laser lines and comparing the results with theoretical calculations as well as with certain characteristics of non-HiPCO nanotubes. We find that the seemingly peculiar spectral features of the HiPCO material can be explained using the existing resonance Raman SWNT theory, and that spectra can be simulated with adequate accuracy by full density of states (DOS) calculations. However, the diameter distribution of the HiPCO sample appears to be rather complex, and the possibility of a non-monomodal Gaussian distribution can not be completely ruled out.

2 Experimental

The HiPCO SWNT material was purchased from Carbon Nanotechnologies Inc. and used without further purification. Preparation of the tubes was performed as outlined in reference [4] with an iron catalyst. Nanotubes synthesized by arc discharge were supplied by Prof. Kataura of Tokyo Metropolitan University, Japan [11] and used for comparison purposes. Samples for the Raman measurements were prepared by drop-coating a hot gold mirror cast on a clean silicon wafer by a tetrahydrofuran suspension of the SWNTs. Prior to the measurements, the samples were heated to 500 K for 12 hours in a vacuum better than 5×10^{-3} Pa to remove traces of leftover solvent and adsorbed contaminants. Raman spectra were recorded at 77 K in vacuum with 9 different lasers extending from 1.83 eV to 2.71 eV (676 nm – 457 nm) with a spectral resolution of 2 cm^{-1}. Analysis and detection of the scattered light was performed with a Dilor xy spectrometer and a liquid N_2 cooled CCD detector.

Theoretical Raman spectra were calculated using the method detailed previously [8] to obtain the Raman cross-sections from total DOS calculations performed within the tight-binding approximation [12].

TEM images were recorded on samples drop dried from diethylether onto a copper grid (3.0 mm, 200 mesh coated with formvar film). The images revealed high sample purity with respect to amorphous carbon particles but clearly demonstrated the presence of metallic particles sticking to the nanotubes, a known feature of the HiPCO process. It has been reported [9] that only certain relative intensities suffer minor changes in the Raman spectrum even after removing these particles by a multi-step acidic-oxidative purification protocol. Therefore, we assume that the presence of leftover iron does not perturb the phonon structure of the SWNTs significantly, thus the application of existing Raman formalism is justified for our raw HiPCO samples as well.

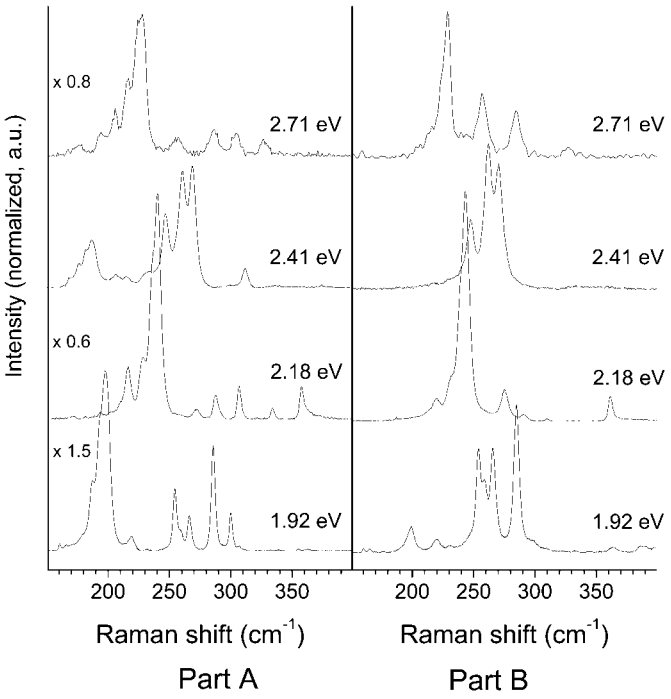

Fig. 1. Radial breathing mode region of the Raman spectra of HiPCO (A) and arc discharge (B) SWNTs of comparable diameters. Scaling factors relative to the intensity of the highest peak in the 2.41 eV spectrum are given in the left side of the figure.

3 Results

Raman spectra as measured at four characteristic laser energies in the radial breathing mode (RBM) window are presented in Figure 1 for both the studied HiPCO and the arc discharge reference material. It is known from a previous analysis that the reference material has a monomodal Gaussian diameter distribution with a center (d_0) at 0.97 nm and a width (σ) of 0.11 nm. The expected oscillatory behavior of the first spectral moment can be readily observed for both samples. Comparing the spectra to those of the HiPCO material, the latter appear more structured and contain additional strong peaks both at low and high wave numbers. This might suggest a more complex diameter distribution, which could be either a broader monomodal Gaussian, a bimodal Gaussian or even non-Gaussian one.

The HiPCO SWNT's G band, a multi-component spectral feature related to the tangential Raman mode in graphite, is presented as hollow squares in Figure 2 for three characteristic laser energies. It is interesting that the shapes of G bands measured with green (2.41 eV) and red (1.83 eV) lasers show an opposite trend compared to spectra recorded for nanotubes grown by conventional methods [13]: the elongated low-energy slope of

Table 1. Line shape analysis of the Raman spectra of the HiPCO material. Center (ω_0) and FWHM (Γ) are listed for all peaks, while additionally the ($1/q$) parameter is given for the Breit-Wigner-Fano features.

	1.83 eV			1.92 eV			2.18 eV		
Peak	ω_0 (cm^{-1})	Γ (cm^{-1})	$1/q$	ω_0 (cm^{-1})	Γ (cm^{-1})	$1/q$	ω_0 (cm^{-1})	Γ (cm^{-1})	$1/q$
1	1531	32		1529	26	−0.12	1524	49	−0.22
2				1544	10		1527	7	
3	1547	12		1554	9		1541	19	
4	1556	10		1561	9		1552	21	
5	1564	10		1582	12		1578	27	
6	1596	11		1594	9		1590	15	
7	1602	18		1600	16		1597	27	
	2.34 eV			2.38 eV			2.41 eV		
1	1524	56	−0.22	1524	53	−0.18	1522	51	−0.24
2	1528	7		1529	9		1528	10	
3	1550	25		1552	25		1549	26	
4	1575	26		1575	22		1571	23	
5	1587	12		1587	11		1582	10	
6	1595	13		1596	12		1593	13	
7	1604	24		1605	20		1602	22	
	2.50 eV			2.60 eV			2.71 eV		
1	1524	54	−0.21	1527	38		1539	17	
2	1525	7							
3	1550	28		1553	26		1563	15	
4	1566	14		1566	14		1571	9	
5	1575	13		1574	13		1591	3	
6	1595	13		1596	13		1595	10	
7	1604	21		1604	22		1601	18	

the 1590 cm^{-1} peak – generally assigned to resonances of metallic nanotubes – appears in the green instead of the red. On the other hand, spectra measured with red lasers are similar to those spectra of SWNT prepared by conventional techniques where the resonance is dominated by semiconducting tubes. We have performed spectral decomposition by fitting the spectra with multiple Voigt area and Breit-Wigner-Fano (BWF) type peaks, indicated by dotted lines in Figure 2. The characteristics of all fitted peaks are summarized in Table 1. The peak with the highest amplitude is always the one between 1590–1600 cm^{-1}, and the absolute intensity of the spectrum is higher in the blue and in the red than in the green. Peaks 3–7 between 1541 cm^{-1} and 1605 cm^{-1} can be associated with the lattice C-C stretching vibrations E_2, A, E_1, respectively, where for each transversal and longitudinal components are possible. The low frequency BWF type peak 1 is attributed to the longitudinal A vibration (A(LO)) of metallic SWNTs [14]. The narrow and low intensity peak 2 appears to be a satellite of peak 1, however, its assignment is not unambiguous at present. The contribution of the BWF line is most pronounced when measured with the lasers 2.41, 2.38, 2.31 and 2.18 eV. The Fano shape is weak but observable at 2.50 eV and 1.92 eV, and is completely absent from the spectra recorded at 2.71 eV, 2.60 eV and

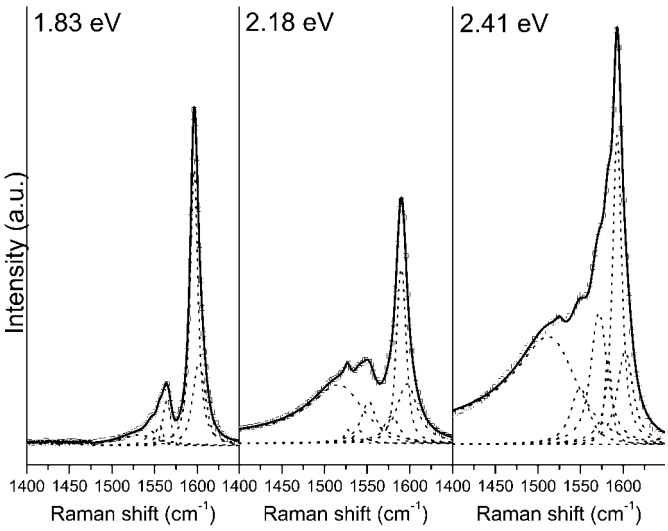

Fig. 2. Typical decompositions of the Raman G band of HiPCO SWNTs. For all three laser energies, hollow squares denote the measured values (every 5th point shown), dotted lines correspond to individual fitted peaks and the solid line marks the envelope of the fitted peaks.

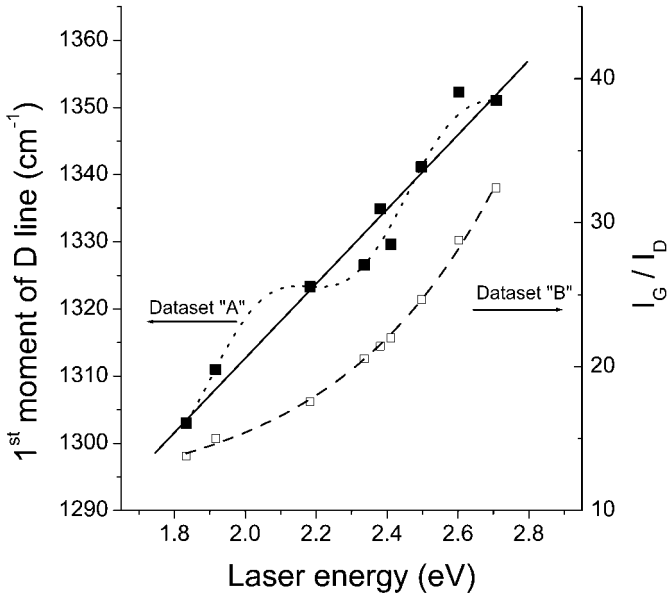

Fig. 3. Excitation energy dependence of the first spectral moment of the Raman D line ("A", left y axis) and the I_G/I_D ratio ("B", right y axis) of the HiPCO samples studied herein. The dotted line marks the sinusoid oscillations of Dataset A, the dashed line shows the exponential curve fitted to Dataset B. See text for parameters of these curves.

1.83 eV. It is remarkable that the position of the BWF peak is downshifted by about 20 cm^{-1} to 1525 cm^{-1} as compared to literature data reported for $d = 1.49 \pm 0.2$ nm arc discharge SWNTs [15] and laser ablation grown tubes with larger diameter [16]. Since the same phenomenon was observed in the arc discharge reference material, the downshift is most likely caused by the diameter dependence of the position of the BWF line and is not specific to the HiPCO process. This downshift is consistent with a recently reported dependence of the BWF line position on tube diameter [15].

Analysis of the other characteristic SWNT Raman feature, the defect-related D line (around 1330 cm^{-1}) has also been performed. Data set "A" (left y axis) in Figure 3 represents the up shift of the D line position with increasing laser energy. For each laser energy the standard error of the D line position was smaller than 0.5 cm^{-1} due to the large signal-to-noise ratio. The up shift is linear to a first approximation (solid line in the figure) with a slope of 55.4 ± 6.5 cm^{-1}/eV – a value typical for well-grown and unfunctionalized SWNTs. Strong etching or functionalization would have decreased the slope to about 35–45 cm^{-1}/eV [17]. Sinusoid oscillations are superimposed on the linear change, and can be quantified by fitting the first moment of the D-line using the formula $m_{1,D-line} = 1215 + 49.7 \times E + 4.7 \sin(11.3 \times E - 2.6)$. The fitted curve is presented as a dotted line in Figure 3. Such oscillatory behavior was first observed for laser ablation grown SWNTs [18] and resembles the oscillations observed for the first and second spectral moment of the radial breathing mode. In detail it originates from a double resonance scattering process of a K-point phonon as evaluated recently for the laser ablation grown tubes [19,20]. The analysis confirms the oscillatory behavior but also predicts an intrinsically noisy behavior as a consequence of the diameter distribution.

The excitation energy dependence of the ratio of the integrated area of the G and D lines, presented as data set "B" in Figure 3 (right y axis) is nonlinear, and can be approximated with adequate accuracy using the formula $I_G/I_D = 10.6 + 0.06 \exp(E/0.46)$. In both formulas, E denotes the laser excitation energy in eV. The HiPCO I_G/I_D ratio itself is higher than 13 for each laser line. The corresponding lower limit for the I_G/I_D ratio of the reference material is 15, indicating that there is no significant difference in the relative amount of defect sites produced by the two methods.

4 Evaluation of spectra

It is well known that each SWNT contributes to the radial breathing mode (RBM) section of the Raman spectrum. The resonance frequency (ν_{RBM}) is calculated as in equation (1), where d is the tube diameter given by equation (2) and $a = 2.46$ Å is the lattice constant of graphite.

$$\nu_{\mathrm{RBM}} = \frac{C_1}{d(n,m)} + C_2 \tag{1}$$

$$d(n,m) = \frac{a}{\pi}\sqrt{n^2 + m^2 + nm}\,. \tag{2}$$

Reported values for C_1 and C_2 are 224...248 cm^{-1} nm and 8...14 cm^{-1}, respectively. Whether the frequency dependence is really observable in the spectrum or not is determined by (i) the amount of such (n,m) SWNTs in the measured sample, and (ii) the Raman cross-section of that nanotube at the applied laser energy. It was recently demonstrated [21] that analyzing the first two spectral moments of the RBM instead of the positions of its individual peaks gives a reliable estimate for the center (d_0) and the width (σ) of the diameter distribution of SWNTs in the sample, provided that this distribution is monomodal and Gaussian. Results of the RBM analysis performed on the HiPCO SWNT sample are presented in Figure 4. The calculated center of the distribution, $\langle d_0 \rangle = 0.98 \pm 0.05$ nm, is in good agreement with our qualitative expectations based on the spectral similarities of the HiPCO and the reference SWNT material ($d_{0,ref} = 0.97$ nm) as presented in Figure 1, and indicates that the majority of HiPCO nanotubes must indeed be rather thin. On the other hand, the width of the distribution, $\langle \sigma \rangle = 0.21 \pm 0.04$ nm is two times larger than that of the corresponding non-HiPCO reference material ($\sigma_{ref} = 0.11$ nm), suggesting that the validity of the monomodal Gaussian distribution model may not be correct and therefore, needs further justification in this case.

The ultimate test to validate decisions about any distribution model is to show that spectra calculated using that model match the experimental data well. Because of the broad and feature-rich nature of the RBM region of

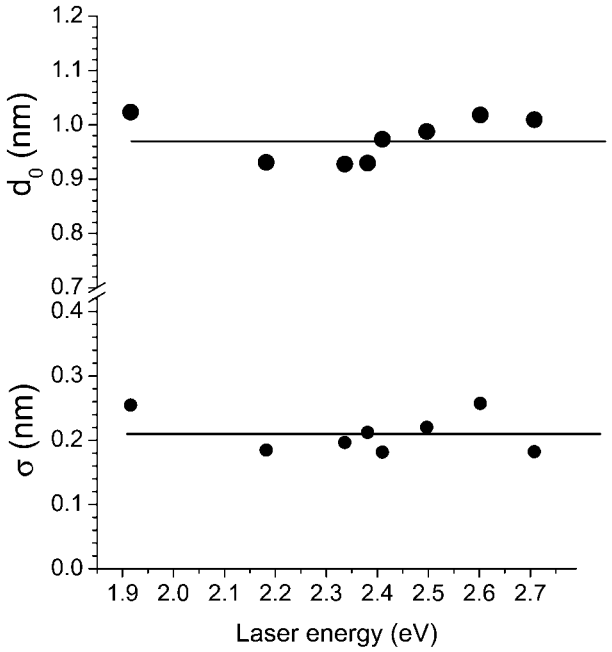

Fig. 4. Center (d_0) and width (σ) of an assumed monomodal Gaussian HiPCO SWNT diameter distribution, as evaluated from the first spectral moment of the measured RBM. Horizontal lines denote the mean values for both quantities: $\langle d_0 \rangle = 0.98$ nm, $\langle \sigma \rangle = 0.21$.

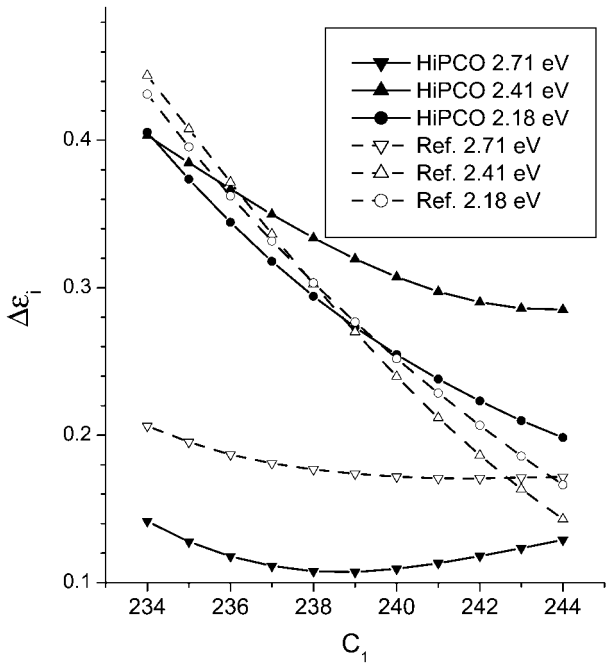

Fig. 5. Effect of modifying C_1 on the logarithmic error sum $\Delta\varepsilon_i$ (as defined in Eq. (3)) of modeling the experimental spectra with a monomodal Gaussian distribution, at three selected laser energies. Full symbols mark calculations for the HiPCO material ($d_0 = 1.05$ nm, $\sigma = 0.15$ nm), empty symbols denote results obtained for the reference material ($d_0 = 0.97$ nm, $\sigma = 0.11$ nm).

the HiPCO Raman spectra, refining the relevant parameters and the parameters of the distribution proved to be a rather challenging task.

A crucial element of such RBM simulations is to chose correct values for the C_1 and C_2 constants in equation (1). Of these two, C_2 describes the tube-tube interaction [22] and is generally assumed a value of 8.5 cm^{-1}. Although theoretical evidence [23] suggests that 234 ± 5 cm^{-1} nm should be used for the scaling constant C_1, values between 223 cm^{-1} nm [24] and 248 cm^{-1} nm [25] have also been reported. Therefore, prior to the simulations of the spectra we have optimized C_1 by minimizing the differences between the measured and the calculated RBMs. The experimentally derived monomodal Gaussian distribution ($d_0 = 0.98$ nm and $\sigma = 0.21$ nm) was used for the tests, and the error ($\Delta\varepsilon$) of the simulation for the ith laser line was defined as:

$$\Delta\varepsilon_i = \frac{1}{N} \sum_{\text{all datapoints}} \log^2 \frac{\alpha_i}{\beta_i} \qquad (3)$$

where α_i and β_i denote the sets of calculated and the measured data points of the spectra for a particular laser energy, and N is the number of data points in a set. Using a logarithmic error sum instead of a conventional squared difference sum was found to be advantageous because it provides error trends more similar to those derived by visual inspection of the spectra. Very close but positively distinct peaks increase the error sum much less in the former as compared to the latter. In Figure 5 the results of the error calculations are presented for three selected laser energies. A minimum at $C_1 = 239$ cm^{-1} nm exists for the 2.71 eV laser, while the error sum is continuously decreasing with increasing C_1 for the 2.41 eV (green) and 2.18 eV (yellow). Our extended analysis has shown that minima exist for these two lasers as well, although they do not fall within the physically meaningful range for C_1. Since the same trends can be observed for the reference SWNTs as well, we assign this behavior to the known shortcomings of the tight-binding model for thin nanotubes. In order to obtain comparable results, a fixed $C_1 = 239$ cm^{-1}nm and $C_2 = 8.5$ cm^{-1} were used in the calculations detailed below.

Concerning the diameter distribution both d_0 and σ were scanned independently over a wide range, with the goal of minimizing the logarithmic error sum as defined in equation (3). Values obtained for certain selected distributions are listed in Table 2, where smaller E values correspond to better fits to the experimental data. The standard error of E (denoted as Ω) is inversely proportional to the ability of the given theoretical distribution to describe spectra measured at all nine laser energies. Parameters of the "original" Gaussian distribution were calculated from the first moment of the RBM (Fig. 4). Besides a monomodal Gaussian also bimodal Gaussians were tested. Both the monomodal and the bimodal Gaussians were found to fit the spectra better than the "original" distribution. The parameter values for the bimodal Gaussian given in Table 2 are typical for several attempts.

Table 2. Adequacy of assumed Gaussian diameter distributions to describe the experimental data at all 9 laser lines. The center and width of the model distributions are given in columns (d_0) and (σ), respectively. Columns E and Ω list the mean error sum and its standard error, respectively.

Model distribution	d_0 (nm)	σ(nm)	E	Ω
Monomodal, original	0.98	0.21	0.49	0.063
Monomodal, improved	1.05	0.15	0.48	0.059
Bimodal, 2:1	0.88 : 1.20	0.05 : 0.07	0.48	0.055

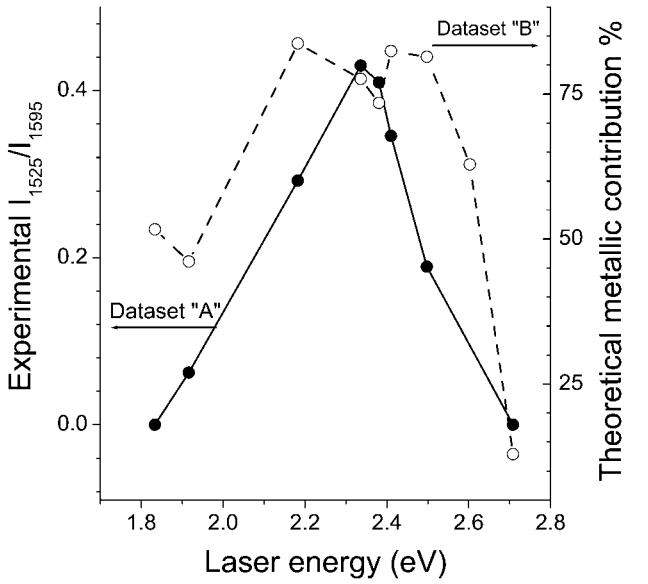

Fig. 6. Relative contribution of metallic HiPCO SWNTs to the total Raman spectrum on the basis of the relative intensity of the Breit-Wigner-Fano peak in the measured G band ("A", full circles), as well as on the basis of tight-binding theoretical calculations ("B", hollow circles).

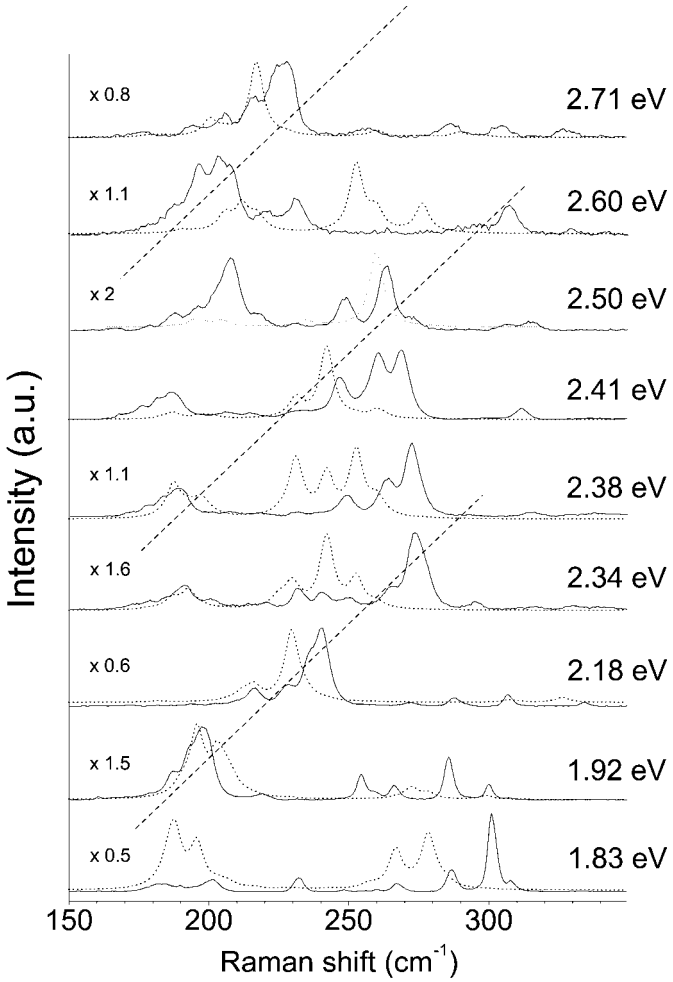

Fig. 7. Comparison of the measured RBM (solid lines) to the RBM calculated (dotted lines) assuming a monomodal Gaussian distribution (d_0 = 1.05 nm, σ = 0.15 nm) at various laser energies. Scaling factors relative to the intensity of the highest peak in the 2.41 eV spectrum are given in the left side of the figure. The thin dashed lines from lower left to upper right are guides for the eye.

As can be seen from the table the gain in fitting quality by using the bimodal Gaussian is rather low. Only the standard error is reduced.

With these improvements some general comparisons of the experiments can be performed with model calculations on the tight binding basis. It is generally accepted [15] to assign the broad ∼1525 cm^{-1} Breit-Wigner-Fano peak and the sharp ∼1595 cm^{-1} component of the G band to resonances of metallic and semiconducting SWNTs, respectively. Therefore, the intensity ratio of these lines is proportional to the amount of metallic tubes brought into resonance at a certain laser energy. On the other hand, the contribution of metallic tubes (M) to the total simulated spectra can also be calculated as defined in equation (4):

$$M = \frac{\sum\limits_{(n,m)|(n-m)mod\,3=0} \eta(n,m) \times A(n,m)}{\sum\limits_{(n,m)} \eta(n,m) \times A(n,m)} \qquad (4)$$

where the $\eta(n,m)$ Raman cross-section is determined by the laser energy and the helicity of the SWNT considered, and the A abundance is calculated from equation (2) and the diameter distribution curve. In Figure 6, results obtained by both methods for the "improved" monomodal distribution are depicted. As these two curves are derived independently, the remarkable similarity expressed in their trends confirms that the full DOS calculation can also handle HiPCO SWNTs if overall relations are considered.

In Figure 7 the experimental (solid lines) spectra are explicitly compared with the results of the "improved"

monomodal simulation (dotted lines). The characteristic grouping into three sets of lines and the up shift of the groups with increasing light energy is very well reproduced by the calculation. With increasing excitation energy these groups shift from the lower left to the upper right. This is indicated by the three dashed lines extending from the lower left to the upper right in the figure and replicates nicely the macroscopic transverse quantization for the distribution of the electronic states. The low frequency group replicates the resonant response between the third van Hove singularities with energy $E_{33}^{(s)}$ in the large diameter semiconducting tubes whereas the high frequency group replicates the resonant response between the second van Hove singularities with energy $E_{22}^{(s)}$ in the small diameter semiconducting tubes. The resonance from the first transition in the metallic tubes at $E_{11}^{(m)}$ can only contribute for laser energies between 1.92 and 2.5 eV and contributes to the central part of the spectrum. Thus, for the observation of the phenomena of macroscopic quantization the HiPCO material is more appropriate than conventional laser ablated or arc discharge tubes. The figure also demonstrates nicely the need of a full evaluation of the Raman spectra if diameter distributions are to be determined. A mere recording of the spectra with 2.71 eV or 2.60 eV laser light would indicate a different mean diameter as compared to a recording with 2.41 eV or 2.34 eV.

Looking into details of the line positions we observe at least a good semi-quantitative agreement between experiment and calculation below 250 cm^{-1} while matches in the high wave number region are harder to find. We expect discrepancies between observed and simulated spectra to get bigger as the diameter of the resonant nanotube decreases. In this case tubes are so thin that the tight-binding simulation is unable to reproduce their density of states well. Whereas line positions are relatively well evaluated for these series by the calculation, the intensity ratios of the spectra are not always reproduced adequately.

The evaluated mean diameters compare well to previous results (*e.g.* 0.79–1.2 nm by Yudasaka *et al.* [26] and 0.8–1.4 nm by Zhou *et al.* [27]) but must be considered as upper limits. As neutron diffraction indicates HiPCO tubes exhibit only weak trends to form bundles [27]. Therefore, the parameter of $C_2 = 8.5$ cm^{-1} used for the intertube interaction might be overestimated, and a smaller value of C_2 would lead to smaller diameters. Widths of Gaussian diameter distributions have not been reported so far to our knowledge. We find both the original value for the width and the width for the improved distribution to be significantly broader than the widths for SWNT grown from conventional processes.

5 Summary

In this paper we discussed the Raman G line, D line and RBM features of a thin SWNT sample synthesized by the new HiPCO process. Experimental results were compared with those obtained for arc-discharge tubes of comparable diameter as well as to calculated spectra. Differences between the Raman spectra of HiPCO and spectra from tubes prepared by conventional techniques originate from two causes: (i) the HiPCO process produces thin tubes, therefore, the metallic resonances are shifted from the red to the green lasers, and (ii) the diameter distribution of the HiPCO sample is not as well defined as that of an *e.g.* arc discharge material. Both a monomodal and a bimodal Gaussian distribution were found to fit the experimental results with almost similar accuracy, indicating that there is no reason to assume complex SWNT diameter distribution functions even in HiPCO materials. Albeit certain high wavenumber peaks in the radial breathing mode region could not be reproduced adequately, the principal features of the HiPCO RBM spectra could be explained on the basis of available resonance Raman theory.

We thank Prof. H. Kataura for providing the reference material and Mag. R. Pfeiffer for experimental assistance. This work was financed through the EU RTN FUNCARS (HPRN-CT-1999-00011).

References

1. S. Iijima, T. Ichihashi, Nature **363**, 603 (1993)
2. C. Journet, W.K. Maser, P. Bernier, A. Loiseau, M.L. De La Chapelle, S. Lefrant, P. Deniart, R. Lee, J.E. Fischer, Nature **388**, 756 (1997)
3. A.G. Rinzler, J. Liu, H. Dai, P. Nikolaev, C.B. Huffman, F.J. Rodriguez-Macias, P.J. Boul, A.H. Lu, D. Heymann, D.T. Colbert, R.S. Lee, J.E. Fischer, A.M. Rao, P.C. Eklund, R.E. Smalley, Appl. Phys. A **67**, 29 (1998)
4. P. Nikolaev, M.J. Bronikowski, K. Bradley, F. Rohmund, D.T. Colbert, K.A. Smith, R.A. Smalley, Chem. Phys. Lett. **313**, 91 (1999)
5. L. Alvarez, A. Righi, S. Rols, E. Anglaret, J.L. Sauvajol, E. Muñoz, W.K. Maser, A.M. Benito, M.T. Martinez, G.F. de la Fuente, Phys. Rev. B **63**, 153401 (2001)
6. S.D.M. Brown, P. Corio, A. Marucci, M.S. Dresselhaus, M.A. Pimenta, K. Kneipp, Phys. Rev. B **61**, R5137 (2000)
7. S. Rols, A. Righi, L. Alvarez, E. Anglaret, R. Almairac, C. Journet, P. Bernier, J.L. Sauvajol, A.M. Benito, W.K. Maser, E. Muñoz, M.T. Martinez, G.F. de laFuente, A. Girard, J.C. Ameline, Eur. Phys. J. B **18**, 201 (2000)
8. H. Kuzmany, W. Plank, M. Hulman, Ch. Kramberger, A. Grüneis, Th. Pichler, H. Peterlik, H. Kataura, Y. Achiba, Eur. Phys. J. B **22**, 307 (2001)
9. I.W. Chiang, B.E. Brinson, A.Y. Huang, P.A. Willis, M.J. Bronikowski, J.L. Margrave, R.E. Smalley, R.H. Hauge, J. Phys. Chem. B **105**, 8297 (2001)
10. L. Kavan, P. Rapta, L. Dunsch, M. J. Bronikowski, P. Willis, R.E. Smalley, J. Phys. Chem. B **105**, 10764 (2001)
11. H. Kataura, Y. Kumazawa, Y. Maniwa, Y. Ohtsuka, R. Sen, S. Suzuki, Y. Achiba, Carbon **38**, 1691 (2000)
12. Ch. Kramberger, S. Bäs-Fischlmair at `http://www.univie.ac.at/spectroscopy/DOS_SWCNT/DOS.html`

13. M.A. Pimenta, A. Marucci, S.D.M. Brown, M.J. Matthews, A.M. Rao, P.C. Eklund, R.E. Smalley, M.S. Dresselhaus, G. Dresselhaus, J. Mat. Res. **13**, 2396 (1998)
14. O. Dubay, G. Kresse, H. Kuzmany, Phys. Rev. Lett. **88**, 235506 (2002)
15. S.D.M. Brown, A. Jorio, P. Corio, M.S. Dresselhaus, G. Dresselhaus, R. Saito, K. Kneipp, Phys. Rev. B **64**, 155414 (2001)
16. A. Kukovecz, unpublished
17. A. Kukovecz, Ch. Kramberger, M. Holzinger, H. Kuzmany, J. Schalko, M. Mannsberger, A. Hirsch, J. Phys. Chem. B **106**, 6374 (2002)
18. A. Grüneis, M.Sc. Thesis, University of Vienna, 2001
19. J. Kürti, V. Zólyomi, A. Grüeis, H. Kuzmany, Phys. Rev. B **65**, 165433 (2002)
20. J. Maultzsch, S. Reich, C. Thomsen, Phys. Rev. B **64**, 121407 (2001)
21. M. Hulman, W. Plank, H. Kuzmany, Phys. Rev. B **63**, R081406 (2001)
22. L. Henrard, Ph. Lambin, A. Rubio, in *Proc. Int. Winterschool on "Electronic Properties of Molecular Nanostructures", Kirchberg, 2000*, edited by H. Kuzmany *et al.*, AIP Conference Proceedings Vol. 544 (Melville, New York, 2000), p. 266
23. J. Kürti, G. Kresse, H. Kuzmany, Phys. Rev. B **58**, R8869 (1998)
24. S. Bandow, S. Asaka, Y. Saito, A.M. Rao, L. Grigorian, E. Ricther, P.C. Eklund, Phys. Rev. Lett. **80**, 3779 (1998)
25. A. Jorio, R. Saito, J.H. Hafner, C.M. Lieber, M. Hunter, T. McClure, G. Dresselhaus, M.S. Dresselhaus, Phys. Rev. Lett. **86**, 1118 (2001)
26. M. Yudasaka, H. Kataura, T. Ichihashi, L.-C. Qin, S. Kar, S. Iijima, Nano Lett. **1**, 487 (2001)
27. W. Zhou, Y.H. Ooi, R. Russo, P. Papanek, D.E. Luzzi, J.E. Fischer, M.J. Bronikowski, P.A. Willis, R.E. Smalley, Chem. Phys. Lett. **350**, 6 (2001)